ChemPubSoc Europe

DOI: 10.1002/celc.201800431

CHEMELECTROCHEM Articles

# Efficient In Situ Utilization of Caustic for Sequential Recovery and Separation of Sn, Fe, and Cu in Microbial Fuel Cells

Liping Huang,*[a] Zheqian Lin,[a] Xie Quan,[a] Qingliang Zhao,*[b] Wulin Yang,[c] and Bruce E. Logan[c]

A novel strategy to sequentially recover and separate Sn(II), Fe(II) and Cu(II) from a synthetic wastewater from printed circuit board (PrCB) manufacturing in a single microbial fuel cell ($MFC_{Sn}$)-$MFC_{Fe}$-$MFC_{Cu}$ process was achieved, where in-situ produced caustic was primarily utilized for Sn precipitation ($MFC_{Sn}$) and then secondly used for Fe deposition ($MFC_{Fe}$) and anaerobic Cu(II) reduction in the final $MFC_{Cu}$. An external resistance of 1000 Ω in the $MFC_{Sn}$ and $MFC_{Fe}$, and a 10 Ω resistor in the $MFC_{Cu}$ achieved predominant recovery of Sn ($MFC_{Sn}$: 80.8 ± 0.8%), Fe ($MFC_{Fe}$: 59.1 ± 0.8%), and Cu ($MFC_{Cu}$: 68.2 ± 1.8%) in the three MFCs, with separation factors of 32.1 ± 1.6 for Sn ($MFC_{Sn}$) and 7.5 ± 1.8 for Fe ($MFC_{Fe}$), and complete recovery of Cu ($MFC_{Cu}$, 42-mesh cathodes). The metal concentrations in the final effluent were below national discharge limits (Sn, 2.0 mg/L; Fe, 5.0 mg/L; Cu, 0.2 mg/L). The metal recoveries ranged from 2.6 (Sn, $MFC_{Sn}$)–12.0 (Cu, $MFC_{Cu}$), and the separation factors were 8.4 (Sn, $MFC_{Sn}$)–∞ (Cu, $MFC_{Cu}$) times those of the open circuit controls. Cathodes with 120-mesh size of stainless steel mesh produced lower metal recoveries [33.7% (Sn, $MFC_{Sn}$) and 27.0% (Fe, $MFC_{Fe}$) decrease] and separation factors than MFCs with 42-mesh cathodes. This study provides a viable approach for efficiently recovering and separating Sn, Fe and Cu from stripping solutions produced in PrCB manufacturing, with simultaneous power production.

## 1. Introduction

Tin (Sn), iron (Fe) and copper (Cu) are using present in stripping solutions that are a by-product of printed circuit boards (PrCBs) manufacturing.[1,2] With the large demand for electronic equipment, the world market for PrCBs reached an estimated $58.6 billion in value in 2015, with Asia accounting for 91% of this production, according to the report from the Institute of Printed Circuits (http://www.ipc.org). As a result, a large volume of stripping solution was generated from PrCB manufacturing processes that included imaging, plating, and etching. The three most abundant metals in these stripping solutions had large ranges of concentrations of 0.002–53 g/L (Sn), 0.7–40 g/L (Cu) and 2.7–25 g/L (Fe), which were similar to or higher than metal concentrations in the original ores.[1–7] Thus, efficient approaches for recovering and separating these metals are needed.

[a] Prof. L. Huang, Z. Lin, Prof. X. Quan
Key Laboratory of Industrial Ecology and Environmental Engineering, Ministry of Education (MOE)
School of Environmental Science and Technology
Dalian University of Technology, Dalian 116024, China
E-mail: lipinghuang@dlut.edu.cn

[b] Prof. Q. Zhao
State Key Laboratory of Urban Water Resource and Environment
Harbin Institute of Technology, Harbin 150090, China
E-mail: qlzhao@hit.edu.cn

[c] Dr. W. Yang, Prof. B. E. Logan
Department of Civil and Environmental Engineering
The Pennsylvania State University
University Park, Pennsylvania, 16802, USA

Supporting information for this article is available on the WWW under https://doi.org/10.1002/celc.201800431

Solvent extraction, chemical precipitation and flocculation, and electrochemical deposition have been typically employed to recover Sn, Cu and Fe from stripping solutions generated from PrCB manufacturing.[1,2,8–10] However, the entire treatment process required pH adjustments by the addition of caustic (0.1–1.0 M), and the operational costs associated with continuous chemical addition or electricity consumption were high. Moreover, the process generated large amounts of sludge that required disposal, and this sludge is normally classified as hazardous due to the high concentration of heavy metals. Cost-effective and environmental friendly approaches for recovery and separation of these metals is therefore desirable.

A microbial fuel cell (MFC) is an emerging technology that has garnered tremendous attention for its ability to simultaneously treat wastewater and produce electrical power.[11–17] Compared to aqueous catholyte in MFCs using single or mixed metals as final electron acceptors, including Cu(II), Cr(VI), V(V), Cd(II), W(VI) and Mo(VI),[18–26] air-cathode MFCs are more promising systems due to higher power production and coulombic efficiency (CE) as well as more sustainability of oxygen as a oxidizer at the cathode.[11,13,14,27] The use of a passive air-cathode requires less energy input for oxygen reduction at the cathodes that use dissolved oxygen, due to the high energy demands needed for air sparging.[11,13,14,27] Inexpensive air-cathodes have been developed for MFC applications due to the use of activated carbon as the catalyst and a stainless steel mesh current collector.[28–30] When separators or membranes are used in MFCs with oxygen reduction at the cathode, caustic can be generated at the cathode (reaction 1).[31–32] This caustic can be in-situ or ex-situ utilized for either removal of phosphorus as struvite from swine wastewater,[33]or recovery of

individual metals such as Cu(II), Fe(III), Zn(II), Cd(II), Co(II),[34–37] and mixed W(VI) and Mo(VI).[38,39] However, the use of caustic has barely been examined for effective treatment of wastewaters from PrCB manufacturing with the requirement of simultaneous recovery and separation of Sn(II), Fe(II) and Cu(II) in a single process.

The production of caustic can be generated in-situ for Sn, Fe and Cu recovery and separation in MFCs, as shown by the reactions [Eqs. (1)–(8)]:

$$O_2 + 2H_2O + 4e^n = 4OH^- \quad E^\theta = +0.401\ V \tag{1}$$

$$Sn^{2+} + 2H_2O = Sn(OH)_2^- + 2H^+ \quad K_{sp} = 1.4 \times 10^{n28} \tag{2}$$

$$2Sn^{2+} + O_2 + 4H^+ = 2Sn^{4+} + 2H_2O \tag{3}$$

$$Sn^{4+} + 4H_2O = Sn(OH)_4^- + 4H^+ \quad K_{sp} = 1.0 \times 10^{n56} \tag{4}$$

$$4Fe^{2+} + 4H^+ + O_2 = 4Fe^{3+} + 2H_2O \tag{5}$$

$$Fe^{3+} + 3OH^n = Fe(OH)_3^- \quad K_{sp} = 2.8 \times 10^{n39} \tag{6}$$

$$Cu^{2+} + 2OH^n = Cu(OH)_2^- \quad K_{sp} = 2.2 \times 10^{-20} \tag{7}$$

$$Cu^{2+} + 2e^n = Cu(s) \quad E^\theta = +0.340\ V_{SHE} \tag{8}$$

Sn and Fe can be produced from crystallization of inorganics in stripping solutions from PrCB manufacturing.[1,3,9] Crystal precipitation occurs when concentrations of Sn(IV), Fe(III) or Cu(II) and caustic exceed the solubility limit for $Sn(OH)_4$ ($1.0\times10^{-56}$), $Fe(OH)_3$ ($2.8\times10^{-39}$) or $Cu(OH)_2$ ($2.2\times10^{-20}$) (Eqs. 2, 4, 6 and 7). Thus, this gravimetric separation of metal precipitates from catholytes is highly dependent on pH and oxygen (Eqs. 3, 5 and 7),[2] resulting in the precipitated $Sn(OH)_4$ near pH = 0.79, $Fe(OH)_3$ at pH = 3.06 and $Cu(OH)_2$ = 5.68. This pH increase could be achieved in air-cathode MFCs due to caustic generation at the cathode,[31–32] with the most easily precipitated Sn(IV) in one MFC unit, followed by Fe(III) precipitation in the second one. For Cu recovery, considering that Cu(0) is more valuable than $Cu(OH)_2$, and that anaerobic conditions favor Cu(II) reduction on the cathode (Eq. 8),[19,21–23] the third MFC can be anaerobically maintained for copper reduction to Cu(0), and thus copper serves as the electron acceptor instead of oxygen.

In this study, a series of three MFC units were examined for metals removal, with the first two having air-cathodes for Sn and Fe precipitation, and the last one using anaerobic conditions for Cu(0) reduction. To optimize metal removal, recoveries were explored under different external resistances and the mesh sizes of stainless steel current collectors were varied in the air-cathodes. The performance of the MFCs was evaluated using linear sweep voltammetry (LSV) and electrochemical impedance spectroscopy (EIS). The metal deposits on the cathodes and the precipitates at the bottoms of MFCs were analyzed by scanning electronic microscopy (SEM), energy dispersive X-ray spectrometry (EDS), and X-ray photoelectron spectroscopy (XPS). System parameters including current, electrode potential, effluent pH and solution conductivity, recovery of Sn, Fe and Cu, coulombic efficiency (CE), and separation factors were used to assess system performance. The results of this study demonstrated a viable approach for efficient recovery and separation of Sn, Fe and Cu from synthetic stripping solutions from PrCB manufacturing with simultaneous electrical power production.

## 2. Results and Discussion

### 2.1. System Performance at an External Resistance of Either 1000 or 10 Ω

A 1000 Ω resistor in the circuit was found to produce better separation of Sn and Fe in the first two MFCs with CEs of 47.0 ± 0.5 %–51.3 ± 0.6 % (24 h cycle) (Table 1), whereas using a 10 Ω in both reactors resulted in metals removal in the first reactor that was too fast to achieve separation of Sn and Fe, and thus both Sn and Fe were removed in the same MFC with higher CEs of 52.8 ± 0.4 %–58.7 ± 0.3 % (5 h cycle) (Figure 1 and Table 1). With the 1000 Ω resistor, the metal precipitation rate of Sn was 16.2 mg/L h in the $MFC_{Sn}$, along with Fe in the $MFC_{Fe}$ (3.0 mg/L h), and then Cu in the third $MFC_{Cu}$ (3.4 mg/L h) for treatment cycles of 24 h (Figure 1A and Figure S1A). With a 10 Ω resistor in all three MFCs, the Sn removal rate was too

**Table 1.** Separation factors ($\varepsilon$) and coulombic efficiencies (CE) in the $MFC_{Sn}$-$MFC_{Fe}$-$MFC_{Cu}$ system.

| Experimental condition | | | $MFC_{Sn}$ | $MFC_{Fe}$ | $MFC_{Cu}$ |
|---|---|---|---|---|---|
| The same 1000 Ω | | $\varepsilon$ | 32.1 ± 1.6 | 7.5 ± 1.8 | +∞ |
| | | CE [%] | 51.3 ± 0.6 | 47.0 ± 0.5 | 37.7 ± 0.6 |
| The same 10 Ω | | $\varepsilon$ | 2.6 ± 0.1 | 1.5 ± 0.4 | +∞ |
| | | CE [%] | 58.7 ± 0.3 | 52.8 ± 0.4 | 41.9 ± 0.6 |
| $MFC_{Sn}$ and $MFC_{Fe}$: 1000 Ω $MFC_{Cu}$: 10 Ω | aerobic-aerobic-anaerobic | $\varepsilon$ | 32.1 ± 1.6 | 7.5 ± 1.8 | +∞ |
| | | CE [%] | 51.3 ± 0.6 | 47.0 ± 0.5 | 43.1 ± 0.0 |
| | anaerobic-anaerobic-aerobic control | $\varepsilon$ | 2.2 ± 0.1 | 0.9 ± 0.1 | +∞ |
| | | CE [%] | 7.3 ± 0.3 | 4.2 ± 0.4 | 56.4 ± 1.5 |
| | 120-mesh cathodes in $MFC_{Sn}$ and $MFC_{Fe}$ | $\varepsilon$ | 11.6 ± 3.7 | 1.1 ± 0.2 | +∞ |
| | | CE [%] | 34.3 ± 1.6 | 32.6 ± 0.5 | 31.0 ± 0.4 |
| | OCC | $\varepsilon$ | 4.1 ± 0.0 | 0.5 ± 0.1 | 0.5 ± 0.2 |
| | | CE [%] | – | – | – |

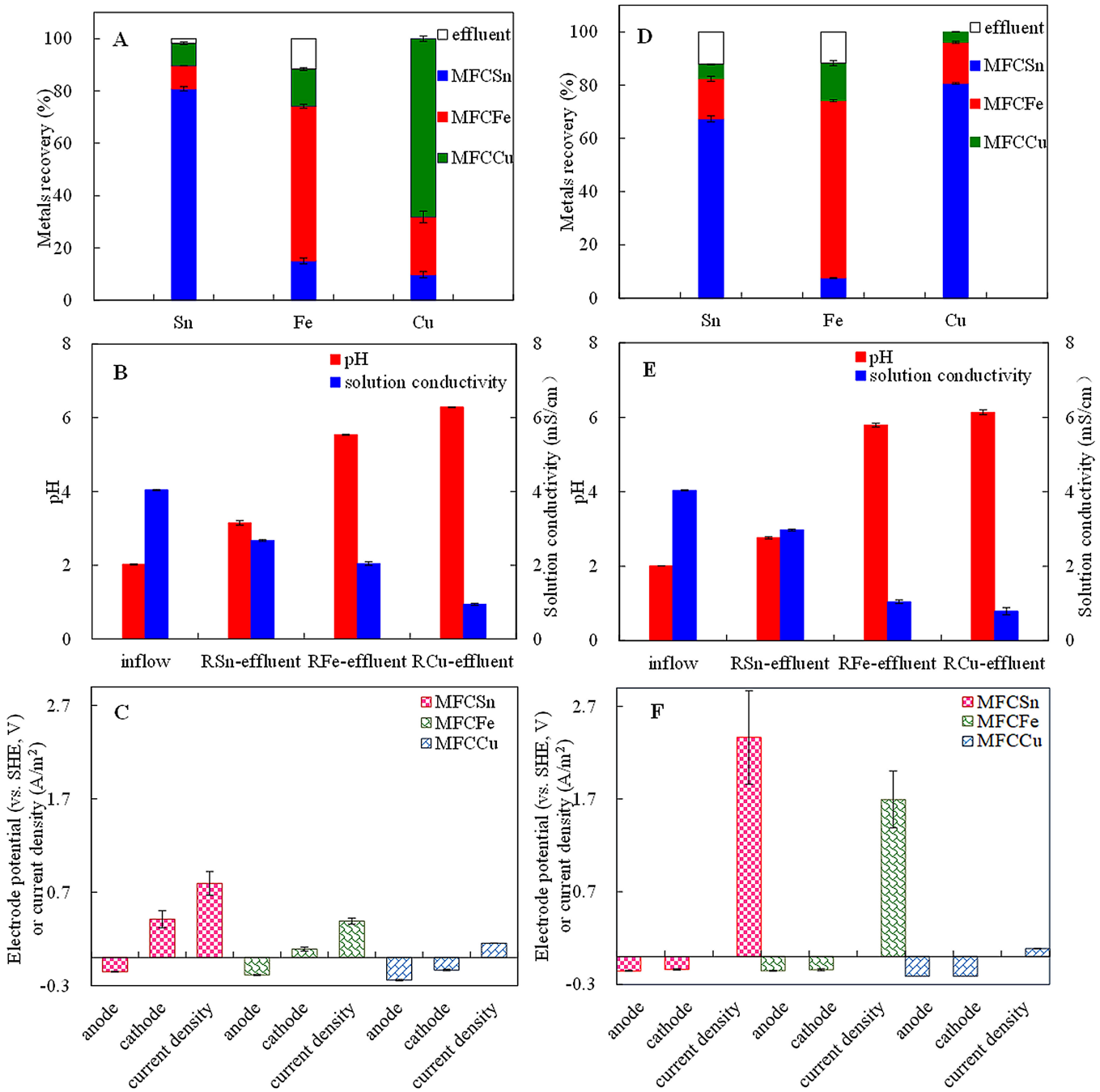


**Figure 1.** Sn, Fe and Cu recovery in the $MFC_{Sn}$-$MFC_{Fe}$-$MFC_{Cu}$ as well as the residual metals in the final effluents (A, D), influent and effluent pHs (B, E), and electrode potentials and current (C, F) at a same 1000 Ω (A–C) (operation time $MFC_{Sn}$: 4 h, $MFC_{Fe}$: 8 h, $MFC_{Cu}$: 12 h) or 10 Ω (D–F) ($MFC_{Sn}$: 1 h, $MFC_{Fe}$: 1.5 h, $MFC_{Cu}$: 2.5 h).

high in the $MFC_{Sn}$ (53.8 mg/L h), along with higher Fe removal (17.8 mg/L h, $MFC_{Fe}$) followed by 48.4 mg/L h of Cu in the $MFC_{Cu}$ for treatment cycles of 5 h (Figure 1D and Figure S1B). These conditions resulted in separation factors of 32.1 ± 1.6 (Sn, $MFC_{Sn}$) and 7.5 ± 1.8 (Fe, $MFC_{Fe}$) at 1000 Ω, which were significantly higher than 2.6 ± 0.1 (Sn, $MFC_{Sn}$) and 1.5 ± 0.4 (Fe, $MFC_{Fe}$) at 10 Ω, despite the same complete Cu recovery at 1000 Ω or 10 Ω.

Conductivities of all effluents similarly decreased at 1000 Ω (Figure 1B and Figure S1B) and 10 Ω (Figure 1E and Figure S1E). However, effluent pH values in all MFCs sequentially increased more at 1000 Ω (Figure 1B and Figure S1B) than at 10 Ω (Figure 1E and Figure S1E), mainly due to more produced $OH^-$ at a much longer operation time in the 1000 Ω. Higher currents were generated with 10 Ω (Figure 1F and Figure S1F) than 1000 Ω (Figure 1C and Figure S1C), similar to previous reports on air-cathode MFCs without metals recovery,[40–41] which resulted in faster metal precipitation. Therefore, a 1000 Ω in the $MFC_{Sn}$ and the $MFC_{Fe}$, and a 10 Ω in the $MFC_{Cu}$ were used for subsequent investigations.

### 2.2. System Performance with $MFC_{Sn}$ and $MFC_{Fe}$ at 1000 Ω, and $MFC_{Cu}$ at 10 Ω

The removal of the metals reached predominant recoveries of Sn (80.8±0.8%) in the $MFC_{Sn}$ and primarily Fe (59.1±0.8%) in the $MFC_{Fe}$ at a total operation period of 12 h (Figure 2A). Using 10 Ω in $MFC_{Cu}$ allowed for nearly complete copper recovery at 3.5 h (68.2±1.8%, 11.7 mg/L h) with a slight increase in CEs compared to other reactors (Figure 2B and Table 1). This copper recovery rate of 11.7 mg/L h at 10 Ω was 3.44 times as that at 1000 Ω in the same $MFC_{Cu}$ (Figure 1A). Moreover, using a low resistance of 10 Ω in $MFC_{Cu}$ also resulted in further Sn and Fe removal, with final effluent concentrations (Sn: 1.4 mg/L; Fe: 4.6 mg/L) below the national discharge limits (2.0 mg/L for Sn, and 5.0 mg/L for Fe) (Figure 2A). In addition, these metal recoveries were 2.57 times (Sn) in $MFC_{Sn}$, 4.43 times (Fe) in $MFC_{Fe}$, and 12.0 times (Cu) in $MFC_{Cu}$, compared to those in the OCC reactors (Figure 2B), reflecting the importance of current generation (CG) for these metal recoveries.

Over each cycle, the pH of the catholyte increased and solution conductivity decreased over time (Figure 2C). The slight increase in effluent pHs (Figure 2D) and decrease in solution conductivities (Figure 2F) for the OCC controls was mainly ascribed to the passive osmosis pressures, resulted from the differences of pH and solution conductivities between the anolyte and the catholyte. The smaller changes for effluent pHs

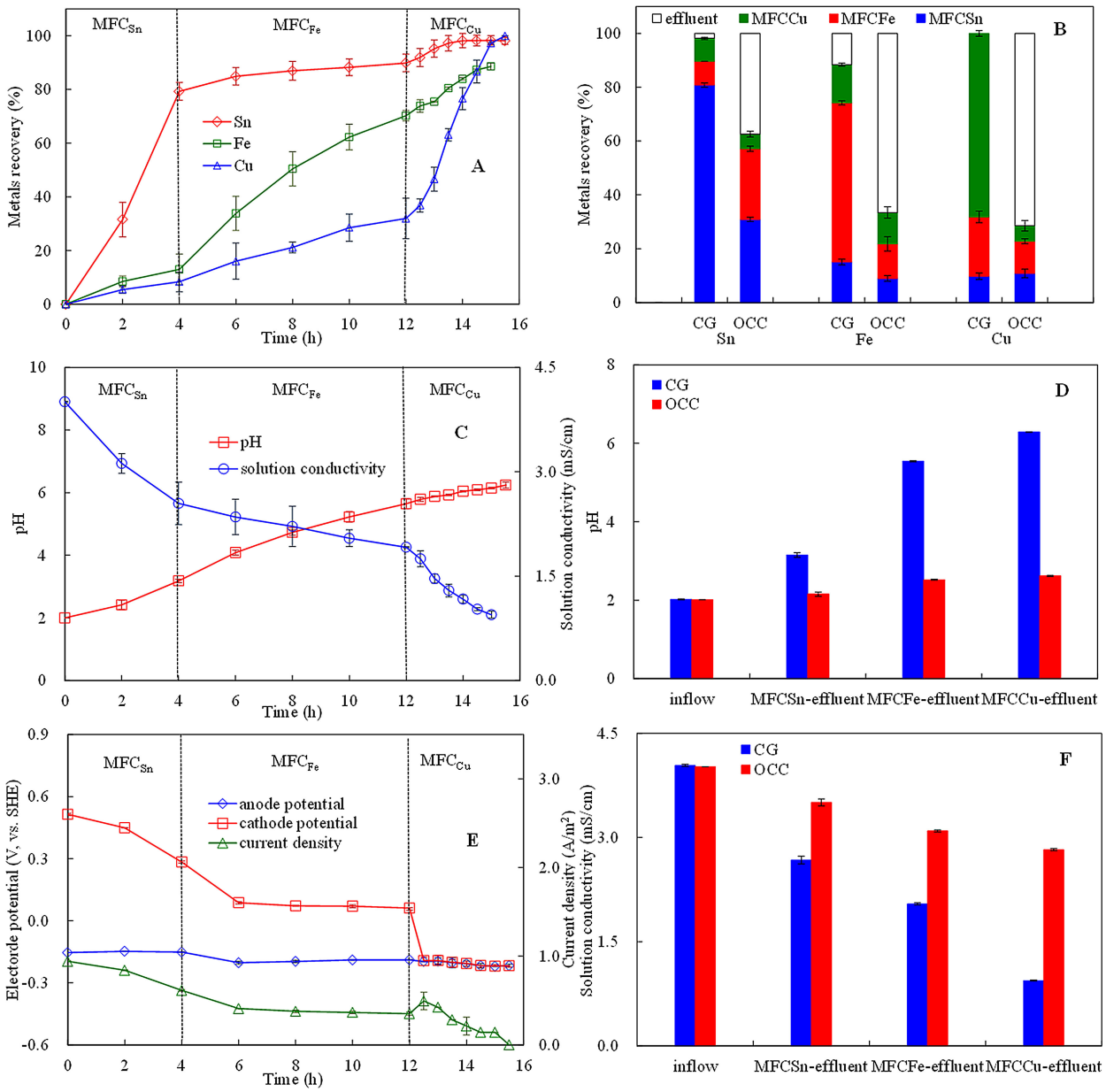


**Figure 2.** Time course of Sn, Fe and Cu recovery in the $MFC_{Sn}$-$MFC_{Fe}$-$MFC_{Cu}$ (A), influent and effluent pHs and solution conductivities (C), and electrode potentials and current densities (E) ($MFC_{Sn}$: 1000 Ω, $MFC_{Fe}$: 1000 Ω, $MFC_{Cu}$: 10 Ω). Comparison of Sn, Fe and Cu recovery in the $MFC_{Sn}$, $MFC_{Fe}$ and $MFC_{Cu}$ as well as the residual metals in the final effluents (B), and influent and effluent pHs (D) and solution conductivities (F) under current generation (CG) or open circuit condition (OCC) (operation time: $MFC_{Sn}$: 4 h, $MFC_{Fe}$: 8 h, $MFC_{Cu}$: 3.5 h).

(Figure 2D) and solution conductivities (Figure 2F) for the OCC controls were in good agreement with the less metal recovery compared to the reactors with current (Figure 2B). Current in the closed circuit MFCs decreased over time (Figure 2E), mainly due to the decrease in metal ions in aqueous solution and the subsequent decrease in solution conductivity (Figure 2C), whereas the decreased cathode electrode potential (Figure 2E) was ascribed to the increased pH (Figure 2C and 2D), and subsequent less $H^+$ ion involvement in the oxygen reduction reaction. Cathode electrode potentials are generally thermodynamically controlled by the reduction reactions on the cathodes, whereas rates of reduction reactions on the cathodes are dynamically influenced by circuit current, which is further a function of the solution conductivity and electrode resistance.[42–44]

### 2.3. Effect of Oxygen

Large differences in Sn and Fe recoveries by the $MFC_{Sn}$ and $MFC_{Fe}$ cathodes were obtained with the two different sizes of stainless steel mesh, but these different conditions did not impact Cu recovery in the third $MFC_{Cu}$. Cathodes with 120-mesh had metal recoveries of 54 ± 5% (Sn) in $MFC_{Sn}$ and 43 ± 4% (Fe) in $MFC_{Fe}$, 34% (Sn in $MFC_{Sn}$) and 27% (Fe in $MFC_{Fe}$) decreases relative to those with 42-mesh cathodes (Figure 3A). Cathodes made from 120-mesh had higher charge transfer and diffusion resistances than the larger mesh size of 42-mesh.[28] The higher diffusion resistance of the 120-mesh accounted for a lower oxygen permeability with an oxygen transfer coefficient of $1.7\times10^{-3}$ cm/s than the $2.2\times10^{-3}$ cm/s of the 42-mesh cathodes,[28] and thus less oxygen was available for subsequent Sn and Fe precipitation.

Separation factors in the effluents of $MFC_{Sn}$ and $MFC_{Fe}$ with 120-mesh cathodes decreased to 11.6 ± 3.7 (Sn, $MFC_{Sn}$) and 1.1 ± 0.2 (Fe, $MFC_{Fe}$) (Table 1). Effluent pH (Figure 3B) and current (Figure 3C) with 120-mesh cathodes followed the same trend of less increase than those with 42-mesh cathodes. Appreciably higher cathode potentials were observed in the $MFC_{Sn}$ and $MFC_{Fe}$ with 42-mesh than 120-mesh cathodes, compared to all the similar anode potentials (Figure 3D), providing evidence that the cathode performance was the reason for the differences in Sn and Fe recovery. In addition, cathode potentials in the $MFC_{Sn}$ were always higher than those in the $MFC_{Fe}$ with either 42-mesh or 120-mesh cathodes. This result was mainly ascribed to the more acidic pH in the influent of $MFC_{Sn}$ (Figure 3B), which was more favorable for oxygen reduction and thus the higher cathode electrode potentials in

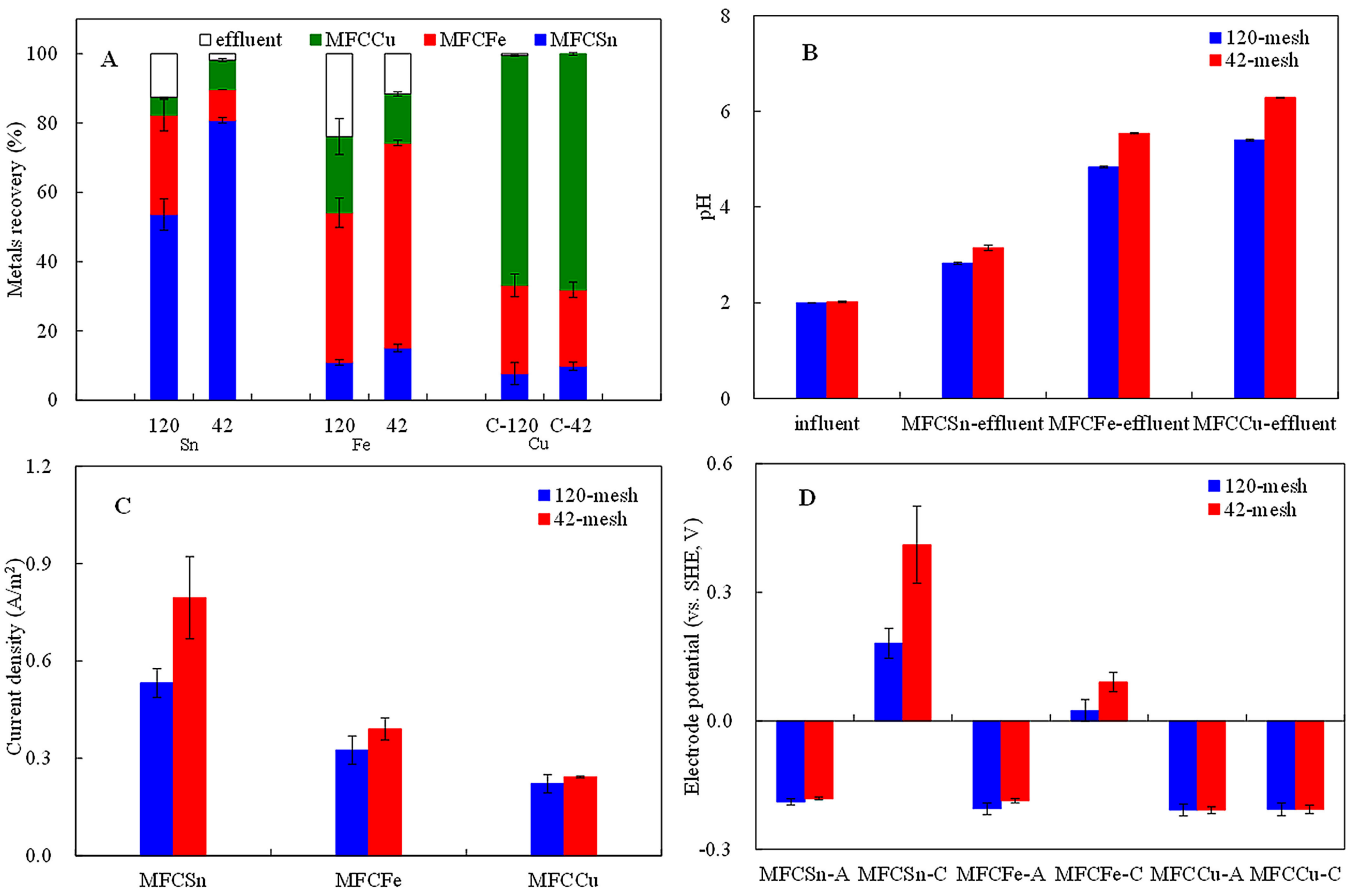


**Figure 3.** Comparison of Sn, Fe and Cu recovery in the $MFC_{Sn}$-$MFC_{Fe}$-$MFC_{Cu}$ as well as the residual metals in the final effluents (A), effluent pHs (B), current (C), and electrode potentials (D) with the $MFC_{Sn}$ and $MFC_{Fe}$ cathodes of 42 (42-mesh) or 120 (120-mesh) mesh sizes of stainless steel mesh ($MFC_{Sn}$: 1000 Ω, $MFC_{Fe}$: 1000 Ω, $MFC_{Cu}$: 10 Ω; $MFC_{Sn}$ operation time: 4 h, $MFC_{Fe}$: 8 h, $MFC_{Cu}$: 3.5 h).

the $MFC_{Sn}$ than those in the $MFC_{Fe}$ (Figure 3D), similar to the situation and our explanation for results in Figure 2C, 2D and 2E. The cathode potentials of $MFC_{Cu}$ were approaching those of the negative anode potentials, due to the very small external resistance of 10 Ω and the low circuit current (Figure 3C), which resulted in low power.

The controls with the anaerobic cathodes in the $MFC_{Sn}$ and $MFC_{Fe}$ reactors, and an air-cathode of $MFC_{Cu}$, all showed decreased metal recoveries (Sn: 20.5 ± 1.1 % in $MFC_{Sn}$; Fe: 19.4 ± 2.4 % in $MFC_{Fe}$; Cu: 29.2 ± 6.9 % in $MFC_{Cu}$) (Figure S2A) compared to the treatment reactors. These lower metal recoveries were consistent with less increase in effluent pH (Figure S2B), lower currents (Figure S2C), and more negative cathode potentials of the $MFC_{Sn}$ and $MFC_{Fe}$ (Figure S2D). The combination of Cu(II) reduction and oxygen reduction resulted in higher currents (Figure S2C), implying the contribution of the binary electron sinks of oxygen and Cu(II) present in the catholyte of the $MFC_{Cu}$ to higher currents, consistent with previous reports in the co-presence of oxygen and either pentachlorophenol, Cu(II) or Co(II).[19,35,45–47] The presence of multiple electron acceptors in the catholyte of MFCs provides more electron sinks for cathodic electrons and resulted in higher currents.[19,47]

### 2.4. SEM-EDS and XPS Analysis

After five cycles with a total operation time of 17.5 h, the precipitates at the bottoms of cathode chambers and on the cathode electrode surfaces of the three MFCs after vacuum drying were quantified by weight, and then analyzed using SEM coupled with EDS. Most of the Sn was recovered from the bottom precipitates (82 ± 5%), with the remainder (18 ± 3%) on the cathodes ($MFC_{Sn}$). For Fe in the $MFC_{Fe}$, 89 ± 4% was precipitated at the bottom and 11 ± 2% on the cathode, but for the Cu in the $MFC_{Cu}$ less Cu was recovered from the bottom precipitates (15 ± 3%) compared to 85 ± 5% on the electrode. The predominant precipitates at the bottoms rather than on the electrodes of $MFC_{Sn}$ and $MFC_{Fe}$ illustrates the advantage of this gravimetric separation for recovery of mixed Sn, Fe and Cu solutions. The greater recovery of copper on the electrode implies the occurrence of more Cu(II) reduction directly on the anaerobic cathodes.

Larger, irregular-shaped aggregates were observed in the $MFC_{Sn}$ (Figure 4A and 4D) than those in $MFC_{Fe}$ and $MFC_{Cu}$ (Figure 4B, 4C, 4E and 4F). The spherical particles at the bottom and on the cathode of $MFC_{Cu}$ (Figure 4C and 4F) was consistent with those in the individual Cu(II)-reduced MFCs.[19,21] The different morphologies of the precipitates from the bottoms (Figure 4A–C) and on the cathodes (Figure 4D–F) may be due to the different cathodic reactions and the subsequent gravity settling processes.[48] EDS analysis of the composition of the agglomerates indicated the similarity of main element composites of the precipitates at the reactor bottom and on the cathodes of each MFCs, but in different ratios (Figure 4G and 4J, 4H and 4K, and 4I and 4L).

The predominant components of the precipitates on the bottom of the reactors and on the cathodes of the three MFCs were examined using XPS spectra (Figure 5) and binding energies for the Sn, Fe and Cu (Table 2). Sn(IV) was present in all reactors based on the characteristic $3d_{5/2}$ at 487.1 ± 0.2 eV and $3d_{3/2}$ at 495.5 ± 0.2 eV (Table 2), for Sn(IV) in $SnO_2$.[2] The existence of Sn(IV) instead of Sn(II) illustrates the occurrence of reactions Eq. 3 followed by Eq. 4, rather than Eq. 2. The primary Sn at the bottom (Figure 5A) was similar to that on the cathode (Figure 5B) of the same $MFC_{Sn}$. There were also Fe and Cu precipitates at the bottom [Fe(III): 91.1 ± 1.4 %, Fe(II): 8.9 ± 1.4 %; Cu(II): 100 %] which were similar to those on the cathode [Fe(III): 90.1 ± 2.8 %, Fe(II): 9.9 ± 2.8 %; Cu(II): 100 %] of the same $MFC_{Sn}$ (Figure S3 and Table 2). The mixed Fe(II) and Fe(III) was consistent with the reported initially formed FeO, and further into $Fe_2O_3$ in the air-cathode MFCs.[36]

Larger differences were observed in the predominant Fe in the $MFC_{Fe}$ (Figure 5C and 5D) and Cu in the $MFC_{Cu}$ (Figure 5E and 5F). There was more Fe(II) (27.7 ± 1.7 %) on the cathode and more Fe(III) (80.7 ± 2.0 %) at the bottom of the $MFC_{Fe}$ (Table 2). For copper, there was Cu(II) (100 %) at the bottom and more Cu(0) (60.4 ± 1.1 %) on the cathode of the $MFC_{Cu}$.

These results demonstrated that Sn(II) was oxidized more readily than Fe(II) in the presence of oxygen (Eqs. 3 and 5), consistent with their thermodynamic calculations.[5] In addition, the cathodic reductive character explains the existence of more reduced precipitates [Fe(II) and Cu(0)] above. Non-predominant precipitates of Sn(IV), Cu(II) (90.1 ± 2.8 %) and Cu(0) (9.9 ± 2.8 %) were obtained from the cathode, compared to only Sn(IV) and Cu(II) in the bottom precipitates of the same $MFC_{Fe}$ (Table 2 and Figure S4). The similar non-predominant precipitates in the bottom precipitates and on the cathode of the $MFC_{Cu}$ [Sn(IV): 100 %, Fe(III): 81.9 ± 1.6 %–82.5 ± 1.4 %, Fe(II): 17.5 ± 1.4 %–18.1 ± 1.6 %] (Table 2 and Figure S5) imply a negligible impact of the anaerobic reductive cathode on these metals.

### 2.5. Long-Term Stability of $MFC_{Sn}$-$MFC_{Fe}$-$MFC_{Cu}$

To assess the stability of the metal deposited cathodes in the three MFCs, the cathodes with previous metal precipitates were used in multiple batch cycles for mixed Sn, Fe and Cu recovery, which were periodically analyzed by EIS and LSV (Figure 6 and Figure S6). A similar trend of deterioration was observed in the three reactors over the 20 cycles, where there was a decrease in the rates of 13.5 % (Sn)–77.3 % (Fe or Cu) in $MFC_{Sn}$ (Figure 6A), 17.4 % (Sn)–59.7 % (Cu) in $MFC_{Fe}$ (Figure 6B), and 13.5 % (Sn)–38.1 % (Cu) in $MFC_{Cu}$ (Figure 6C) compared to cycle 1. These results show the instability of the metal deposited cathodes over repeated cycles. The general trends in current with LSVs were consistent with the performances of those MFCs, as accumulated metals on the cathodes adversely affected current densities and voltages needed to initiate substantial currents (Figure S6). These negative effects could be attributed to an excessive accumulation of metals on the electrodes, which was further shown as follows.

The EIS spectra were fitted to equivalent circuits (Figure S7) to identify the components of the internal resistances in these MFCs after the 2nd, 10th and 20th cycle. Solution resistances

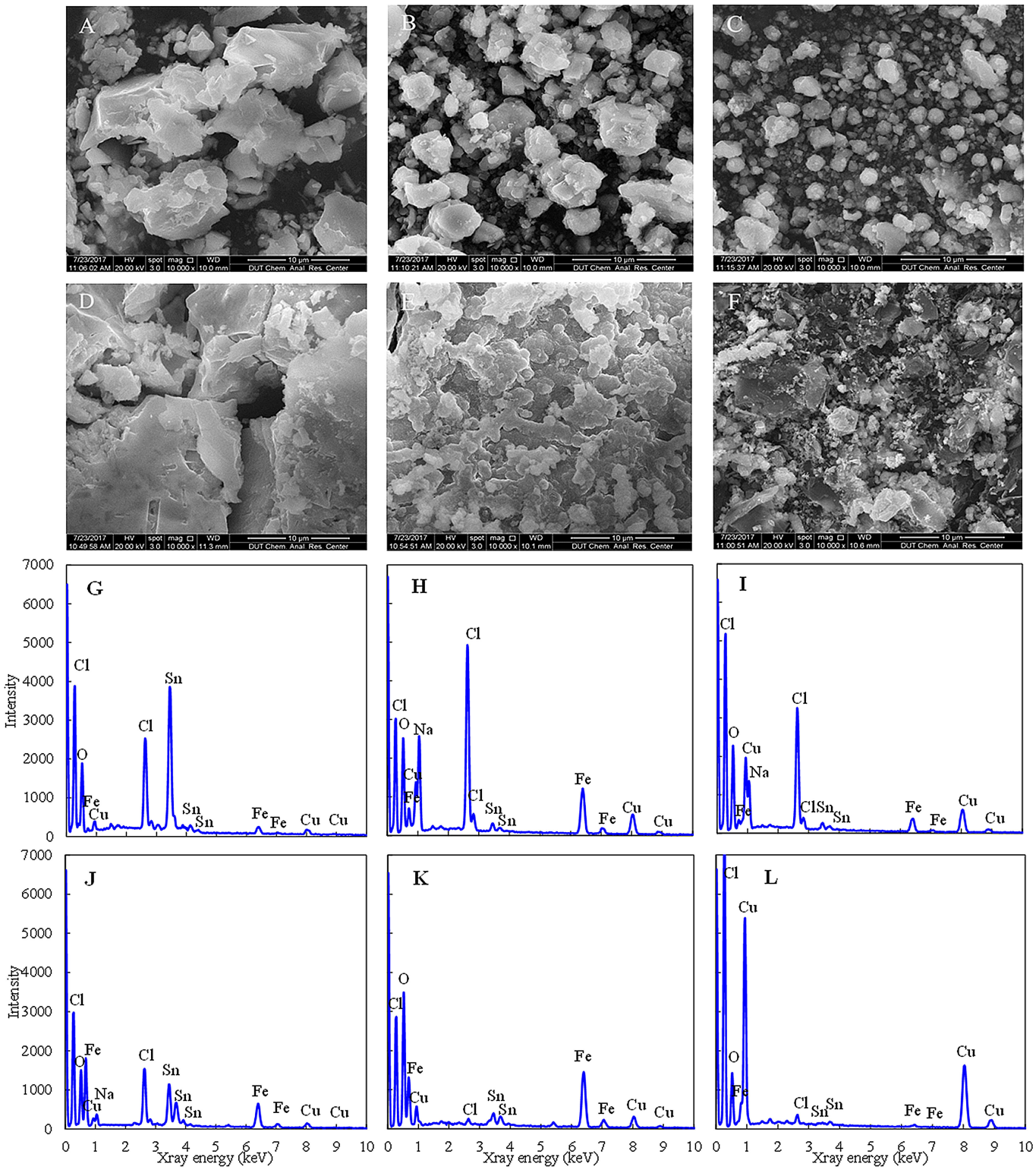


**Figure 4.** SEM observation (A–F) and EDS analysis (G–L) for the precipitates either at the bottoms (A–C, G–I) or on the cathodes (D–F, J–L) of $MFC_{Sn}$ (A, D, G, J), $MFC_{Fe}$ (B, E, H, K), and $MFC_{Cu}$ (C, F, I, L) (5 fed-batch cycles operation).

($R_s$) were all similar for all the cathodes of MFCs and only slightly increased over repeated cycles (Table S1). The diffusional resistance ($R_d$) in all three cathodes was significantly higher than the $R_s$ and the $R_{ct}$, and increased with different extents over time (Table S1), likely due to mass transfer limitations with the formation of the metal precipitates on the electrode. This increased resistance has also be shown in other studies with W and Mo deposited on stainless steel sheet

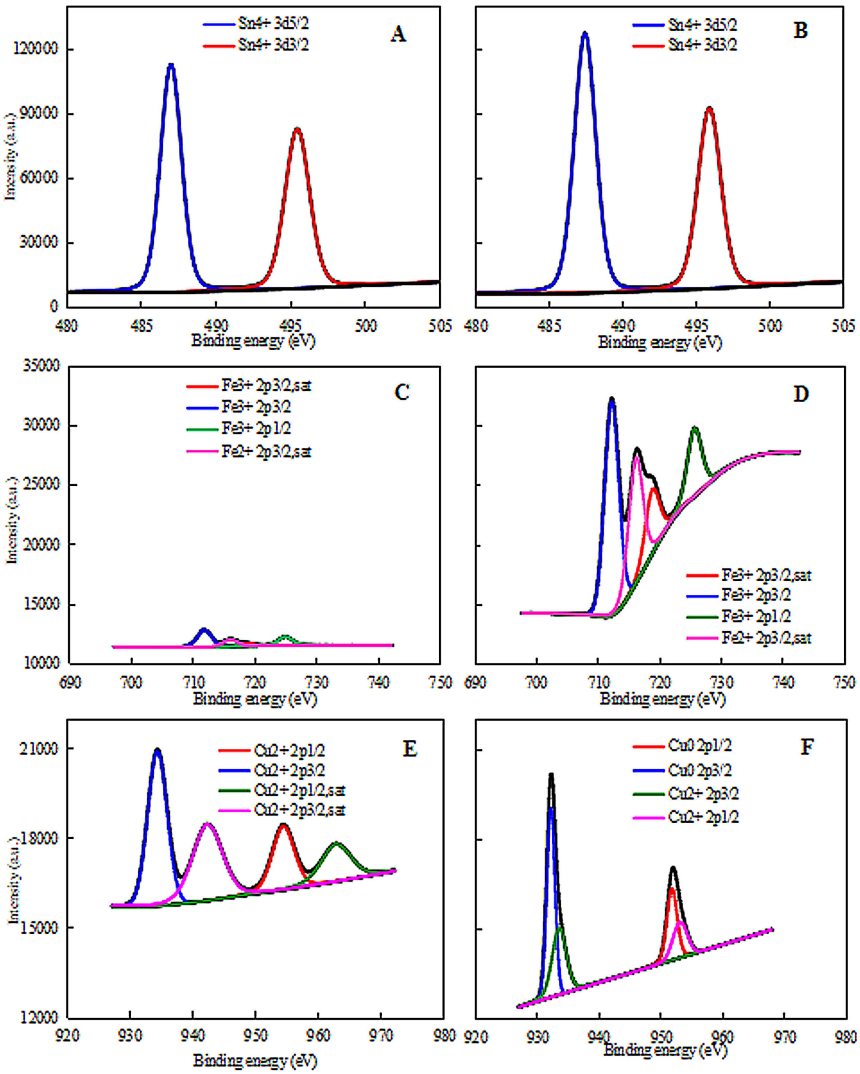


**Figure 5.** XPS analysis for main components in precipitates either at the bottoms (A, C, E) or on the cathodes (B, D, F) of $MFC_{Sn}$ (A, B), $MFC_{Fe}$ (C, D) or $MFC_{Cu}$ (E, F) (5 fed-batch cycles operation).

cathodes in bioelectrochemical systems,[26] Cd deposits on carbon rods or titanium sheets in cathodes of microbial electrolysis cells,[23] and even inorganic precipitates on Pt-free cathodes of MFCs.[49]

### 2.6. Overall Analysis

The results presented in this study demonstrated the critical role of external resistance and oxygen transfer due to the stainless-steel mesh sizes in air-cathode MFCs for efficient in-situ utilization of caustic generated for recovery and separation of Sn, Fe and Cu. Thus, this three-MFC configuration could provide a useful approach for metals recovery from stripping solutions used for PrCB manufacturing, along with simultaneous electricity generation. A high resistance (1000 Ω) in all MFCs ($MFC_{Sn}$-$MFC_{Fe}$-$MFC_{Cu}$) was favorable for Sn and Fe separation, but unsuitable for metal precipitation rates. By using a low 10 Ω, there was accelerated metal precipitation but insufficient Sn and Fe separation. The optimum conditions were using a high resistance (1000 Ω) in the $MFC_{Sn}$ and $MFC_{Fe}$, and a low resistance (10 Ω) in the $MFC_{Cu}$. This mixture of resistances in the reactors not only achieved higher separation factors but also accelerated the copper recovery rates, with the residual metals in the final effluent below the national discharge limits of 2.0 mg/L for Sn, 5.0 mg/L for Fe, and 0.2 mg/L for Cu. Stainless steel mesh with small opening size of 120-mesh in the air-cathodes diminished metal recovery, compared to results with the 42-mesh cathodes. In terms of metal recovery and separation, the importance of external resistance and cathode oxygen permeability, as shown in this study, have been largely overlooked in previous studies.[21–26] Thus, this current study provides better strategies to improve the performance of MFCs as an efficient technology for metal recovery and separation from stripping solutions from PrCB manufacturing.

In previous studies, most of the metals removed have been reductively deposited rather than chemically precipitated on the cathode.[19,21–26,38–39,47–55] The separation of Sn, Fe and Cu

**Table 2.** Composite of various valence states of Sn, Fe and Cu in the $MFC_{Sn}$-$MFC_{Fe}$-$MFC_{Cu}$ system.

| Reactor | Location | $Sn3d_{5/2}$ $Sn^{4+}$ | $Sn_{3d3/2}$ $Sn^{4+}$ | $Fe_{2p3/2}$ $Fe^{3+}$ | $Fe_{2p3/2,sat}$ $Fe^{3+}$ | $Fe^{2+}$ | $Fe_{2p1/2}$ $Fe^{3+}$ | $Cu_{2p3/2}$ $Cu^{2+}$ | $Cu^0$ | $Cu_{2p3/2,sat}$ $Cu^{2+}$ | $Cu_{2p1/2}$ $Cu^{2+}$ | $Cu^0$ | $Cu_{2p1/2,sat}$ $Cu^{2+}$ | Area of Sn [%] $Sn^{4+}$ | Area of Fe [%] $Fe^{3+}$ | $Fe^{2+}$ | Area of Cu [%] $Cu^{2+}$ | $Cu^0$ |
|---|---|---|---|---|---|---|---|---|---|---|---|---|---|---|---|---|---|---|
| $MFC_{Sn}$ | bottom | 487.0 | 495.4 | 711.6 | 718.8 | 716.0 | 724.9 | 933.4 | – | 942.3 | 953.6 | – | 962.1 | 100.0 | 91.1 ± 1.4 | 8.9 ± 1.4 | 100.0 | – |
| | cathode | 487.4 | 495.8 | 711.4 | 718.7 | 716.2 | 725.1 | 933.4 | – | 942.3 | 953.6 | – | 962.2 | 100.0 | 90.1 ± 1.6 | 9.9 ± 1.6 | 100.0 | – |
| $MFC_{Fe}$ | bottom | 487.0 | 495.5 | 711.7 | 718.7 | 716.0 | 725.0 | 933.4 | – | 942.4 | 953.5 | – | 962.1 | 100.0 | 80.7 ± 2.0 | 19.3 ± 2.0 | 100.0 | – |
| | cathode | 487.3 | 495.7 | 711.8 | 718.7 | 716.0 | 725.5 | 933.4 | 932.0 | – | 953.6 | 951.8 | – | 100.0 | 72.3 ± 1.7 | 27.7 ± 1.7 | 90.1 ± 2.8 | 9.9 ± 2.8 |
| $MFC_{Cu}$ | bottom | 486.9 | 495.4 | 711.1 | 718.8 | 716.1 | 725.1 | 934.0 | – | 942.3 | 954.0 | – | 962.5 | 100.0 | 81.9 ± 1.6 | 18.1 ± 1.6 | 100.0 | – |
| | cathode | 486.9 | 495.4 | 711.0 | 718.8 | 716.0 | 725.0 | 933.4 | 932.1 | – | 953.0 | 951.7 | – | 100.0 | 82.5 ± 1.4 | 17.5 ± 1.4 | 39.6 ± 1.1 | 60.4 ± 1.1 |

metals on the electrodes of MFCs represents a challenge for the practical applications of this technology. However, here the metal deposits were mostly in the precipitates for the Sn and Fe metals (82 ± 5% in $MFC_{Sn}$; 89 ± 4% in $MFC_{Fe}$). This sedimentation would facilitate collection of the metals, and thus lower the cost of subsequent metal collection, compared to metals on the electrodes.

Metal deposits on the cathodes can reduce the activity of the electrodes over time, requiring removal of the deposits from the electrodes periodically. This accumulation of metals could represent a challenge for the practical application of this technology. However, the in-situ utilization of these deposits for electrocatalytic or photocatalytic processes may become an attractive strategy for reuse, since Sn, Cu and Fe exhibits excellent electrocatalytic and photocatalytic properties.[56–57] While the present study used a synthetic wastewater to mimic PrCB wastewaters, and the use of actual wastewaters from PrCB manufacturing should be evaluated as well. Practical implementation of this technology will also depend on the long-term operation of this system and other characteristics of the wastewaters, as well as the cost of the system relative to conventional treatment processes. The costs of the materials used in MFCs continues to decrease,[30,42,52] but at this point in time it is likely that this technology is not yet ready for commercial applications as larger-scale studies would be required for evaluating the process prior to commercial and full-scale applications.

## 3. Conclusions

Air cathodes with in-situ produced caustic were used for the first time to sequentially recover and separate Sn, Fe and Cu in a three-MFC system ($MFC_{Sn}$-$MFC_{Fe}$-$MFC_{Cu}$ system). The best performance was obtained with a high resistance (1000 Ω) in $MFC_{Sn}$ and $MFC_{Fe}$, and a low resistance (10 Ω) in the $MFC_{Cu}$. For these conditions, there was faster metal recovery and higher metal separation factors, with the residual metals in the final effluent below the national discharge limit. Cathodes with 120-mesh size of stainless steel mesh diminished metal recovery and separation factor, compared to those 42-mesh size cathodes. These results show this $MFC_{Sn}$-$MFC_{Fe}$-$MFC_{Cu}$ system can be used for efficient Sn, Fe and Cu recovery and separation with simultaneous electricity generation. Since Sn, Fe and Cu are extensively detected in the stripping solutions of PrCB manufacturing, this study provides a viable environmentally benign approach for efficient remediation of stripping solutions contaminated sites with simultaneous production of renewable electricity.

## Experimental Section

### MFC Construction

Dual-chamber MFCs each 4 cm long and with 3 cm diameter chambers were used in all experiments, and every three MFC units

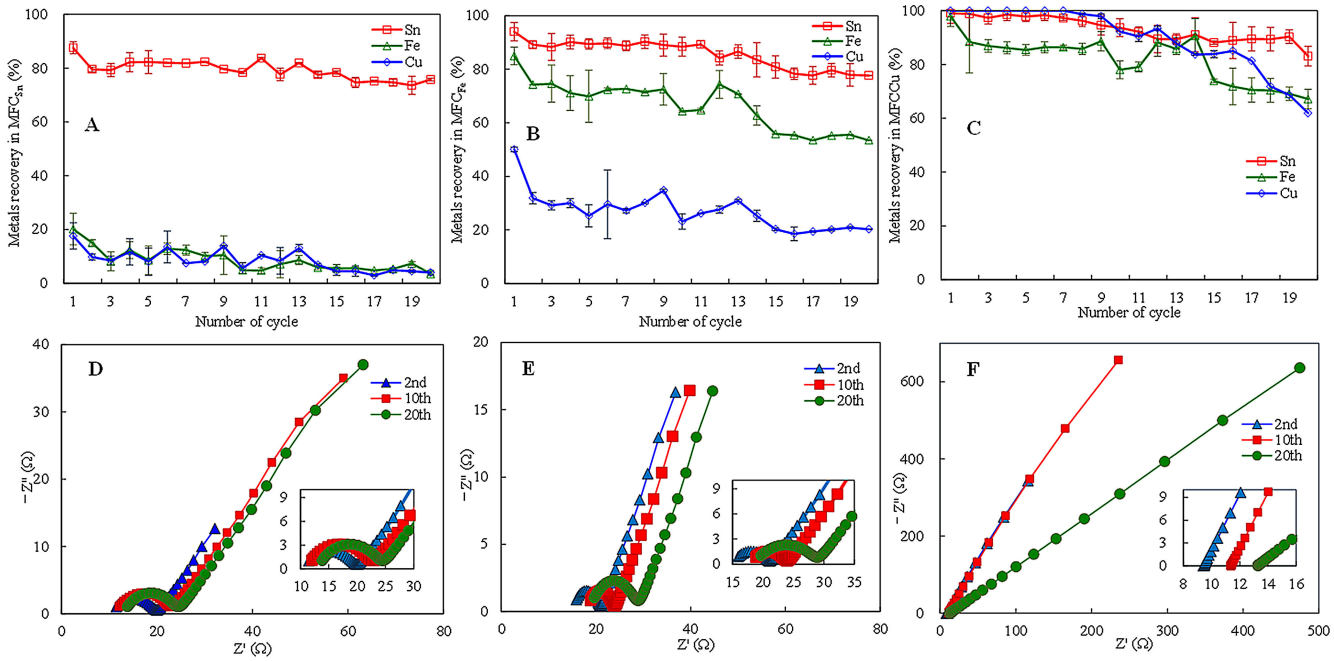


**Figure 6.** Metal recovery (A–C) and Nyquist plots of EIS spectra (D–F) of $MFC_{Sn}$ (A, D), $MFC_{Fe}$ (B, E), and $MFC_{Cu}$ (C, F) as a function of operational cycle. Symbols in (D)–(F) represent experimental data, and lines represent data fit with the equivalent circuit.

were sequentially used to complete one cycle for recovery and separation of mixed Sn(II), Fe(II) and Cu(II). A membrane separator was needed as a barrier to maintain the pH difference between the bioanode and the cathode of each MFC unit, where the bioanode was preferably operated at near neutral pH, and the cathode was sequentially fed with mixed metals effluent from the cathode of the previous MFC unit. An anion exchange membrane (AEM) can selectively transport anions from one side of the membrane to the other, similar to the preferable cation exchange membrane (CEM) for cation ion migration.[14,58–59] Despite the fact that bipolar membranes can achieve less cross-over for anions and cations, they have high voltage losses and thus could not be used as effectively for energy-efficient metal recovery.[19,60] Conversely, the use of non-ion selective separators can minimize pH imbalances, but then all chemicals could cross between the chambers.[61] As a compromise, and considering the acidic mixed anion metals, and durability and cost of ion exchange membrane,[59,61–64] an AEM (Ultrex AMI-7001, Membranes International, Glen Rock, NJ) rather than CEM was used here to separate the two chambers of each MFC unit. Porous graphite felt (1.0×1.0×1.0 cm, Sanye Co., Beijing, China) was used for the anodes of all MFC units. Air-cathodes used in two of the MFCs were made of activated carbon (AC) by sandwiching a catalyst layer of AC (Norit SX plus, Norit Americas Inc., TX) and PTFE (polytetrafluoroethylene) (Sigma Aldrich, USA) between stainless steel mesh (type 304 SS, McMaster-Carr, OH) and a hydrophobic PVDF (polyvinylidene fluoride) membrane diffusion layer (0.45 μm, MILLIPORE, USA).[29–30] Briefly, the AC catalyst layer was prepared by mixing active carbon and a 60% PTFE (polytetrafluoroethylene) emulsion (Sigma Aldrich, USA) in ethanol at a mass ratio of AC/PTFE = 6:1 (6 g AC to 0.67 mL PTFE solution) with stirring on a hot plate at 60 °C. The mixture was continuously stirred at 60 °C to form a gel. The gel was pressed under $1\times10^7$ Pa for 2 s at 60 °C and folded for a second pressing, which was repeated for a total of three times. The prepared AC layer had a thickness of 780 ± 60 μm. The AC catalyst layer was then placed between a precut stainless-steel mesh and hydrophobic PVDF membrane and rinsed with ethanol, pressed at $3\times10^7$ Pa for at least 15 s at 60 °C (Model 4388, CARVER, INC., USA), and dried in a fume hood for 24 h. This cathode was then assembled in the cathode chambers of MFCs with the stainless-steel mesh side to the catholyte and the PVDF side to the air. Two mesh sizes of stainless steel mesh of 42×42 (42-mesh) and 120×120 (120-mesh) (type 304 SS, McMaster-Carr, OH) were used. Mesh characteristics of openings per linear inch, wire diameter, opening size and fractional open area were specified by the manufactures.[28] The cathode of the third MFC unit was a carbon rod, and this MFC was anaerobically operated to reduce Cu(II) to Cu(0).[21–23] The working volume of the anodic and cathodic chambers of each MFC was 25 mL.

## MFC Operation

Anodes were fully pre-acclimated by used MFCs for one month at a fixed external resistance of 1000 Ω.[21–25] The anolyte (pH = 5.8) contained 1.0 g/L sodium acetate dissolved in a phosphate buffer solution (5 mM $NaH_2PO_4$) that was amended with 12.5 mL/L minerals and 5 mL/L vitamins.[24–26,35] A synthetic PrCB waste stripping solution composed of Sn(II) of 80 mg/L, Fe(II) of 40 mg/L and Cu(II) of 60 mg/L was used as initial catholyte influent. The influent pH of the catholyte was set at 2.0, consistent with the acidic condition of the stripping solution from PrCB manufacturing.[2–4] Initial solution conductivities were adjusted to be 4.0 mS/cm using KCl. The amount of the KCl addition was much lower and not enough for its observation on the electrode (Figure 4). This catholyte influent was fed into the air-cathodes of the first MFC. The effluent from the first MFC was then sequentially fed into the second air-cathodes of MFC unit. The effluent of the second MFC was bubbled with ultra-pure $N_2$ for 10 min before filled into the third anaerobic MFC unit. Since Sn(II) is easily oxidized to Sn(IV), which is appreciably easily precipitated than Fe(II) and Fe(III) precipitation, and followed by Cu(II) (Eqs. 4, 6 and 7), the first MFC unit with a shorter operation time was more apt for Sn(IV) precipitates ($MFC_{Sn}$), followed by Fe(II) and Fe(III) precipitates in the second one ($MFC_{Fe}$). The third anaerobic MFC was used for Cu(II) reduction on the cathode ($MFC_{Cu}$).[19,21–23]

MFCs were initially all operated at the same external resistance (1000 Ω or 10 Ω). The more optimal resistance was then identified for each MFC, and then these optimum resistances were used in all subsequent experiments. Air-cathodes using 42-mesh or 120-mesh stainless steel assembled in the $MFC_{Sn}$ and $MFC_{Fe}$ were compared for the impact on system performance as mesh size impacts the amount of oxygen transfer into the catholyte.[28]

Control experiments under open circuit conditions (OCC) were performed to evaluate the impact of current generation (CG) on the system performance. Another set of controls were operated with all completely anaerobic $MFC_{Sn}$ and $MFC_{Fe}$, coupled with an air-cathode $MFC_{Cu}$, to determine the impact of the presence or absence of oxygen on metal recoveries. For anaerobic conditions, the $MFC_{Sn}$ and $MFC_{Fe}$ reactors were operated in an anaerobic glove box (YQX-II, Xinmiao, Shanghai). The aerobic $MFC_{Cu}$ was operated with an air-cathode with 42-mesh stainless steel instead of the carbon rod cathode. All reactors were operated in fed-batch mode at room temperature (22±3 °C) and all experiments were conducted in duplicate.

### Measurements

Sn, Fe and Cu in the influent and effluent of the catholytes were measured using atomic absorption spectroscopy (AAnalyst 700, PerkinElmer). The pH was measured by a calibrated pH meter (PHS-3C, Leici, Shanghai) and the solution conductivity was measured using a conductivity meter (DDS-307, Leici, Shanghai).

The morphology of the metal precipitates and their elemental composition were examined using a scanning electronic microscope (SEM) (QUANTA450, FEI company, USA) equipped with an energy dispersive spectrometer (EDS) (X–MAX, Oxford Instruments, UK). The valences of metal precipitates at the bottoms and on the electrodes were confirmed using X-ray photoelectron spectroscopy (XPS, Kratos AXIS Ultra DLD).

The cathode and anode potentials were monitored by an automatic data acquisition system (PISO-813, Hongge Co, Taiwan). Polarization and power density data were obtained with a potentiostat (VSP, BioLogic) using linear sweep voltammetry (LSV). EIS was conducted using the same potentiostat with a three-electrode system comprising a working electrode (i.e., cathode), a Ag/AgCl reference electrode (195 mV vs. SHE) located 1 cm away from the cathode in the cathodic chamber, and a Pt foil (2×4 cm) counter electrode placed in the anodic chamber. Electrical impedance spectroscopy (EIS) analysis was conducted at cathode potentials under OCCs with either the bare electrodes, or the electrodes deposited with the metal precipitates. EIS frequency ranged from 100 kHz to 10 mHz, with a sinusoidal perturbation of 10 mV amplitude.[24,28,38] The equivalent circuits and detailed values of different resistances were obtained through Zsimpwin software and normalized to the projected area of the cathodes.

The statistical significance of the experimental data was assessed using a statistical package (SPSS v.19.0) (t-test, $p = 0.05$).

### Calculations

Recovery of Sn(II), Fe(II), and Cu(II) in the MFCs was calculated either as shown in Equations (9)–(11) based on the total metal removal (%) or the rate of removal, based on the influent and effluent metal concentrations divided by operation time (mg/L h), in order to provide a systematic assessment for system performance.

$$r_{x,Sn} = \frac{C_{x,Sn,inf} - C_{x,Sn,eff}}{C_{x,Sn,inf}} \times 100\% \quad (9)$$

$$r_{x,Fe} = \frac{C_{x,Fe,inf} - C_{x,Fe,eff}}{C_{x,Fe,inf}} \times 100\% \quad (10)$$

$$r_{x,Cu} = \frac{C_{x,Cu,inf} - C_{x,Cu,eff}}{C_{x,Cu,inf}} \times 100\% \quad (11)$$

where $C_{x,Sn,inf}$ and $C_{x,Sn,eff}$, $C_{x,Fe,inf}$ and $C_{x,Fe,eff}$, $C_{x,Cu,inf}$ and $C_{x,Cu,eff}$ are concentrations of Sn, Fe and Cu in the influent and effluent of each $MFC_x$ unit (x = Sn, Fe, or Cu), and 0.5 is the equivalent constant of the other two non-predominant components relative to the primary component. Separation factors of Sn in the $MFC_{Sn}$ ($\varepsilon_{Sn}$), Fe in $MFC_{Fe}$ ($\varepsilon_{Fe}$) and Cu in $MFC_{Cu}$ ($\varepsilon_{Cu}$), were used to evaluate the extent of removal of each primary component separated from the other non-predominant metals, using Equations (12)–(14):[65]

$$\varepsilon_{Sn} = \frac{(1 - 0.5 \times r_{Sn,Cu} - 0.5 \times r_{Sn,Fe}) \times r_{Sn,Sn}}{(0.5 \times r_{Sn,Cu} + 0.5 \times r_{Sn,Fe}) \times (1 - r_{Sn,Sn})} \quad (12)$$

$$\varepsilon_{Fe} = \frac{(1 - 0.5 \times r_{Fe,Sn} - 0.5 \times r_{Fe,Cu}) \times r_{Fe,Fe}}{(0.5 \times r_{Fe,Sn} + 0.5 \times r_{Fe,Cu}) \times (1 - r_{Fe,Fe})} \quad (13)$$

$$\varepsilon_{Cu} = \frac{(1 - 0.5 \times r_{Cu,Sn} - 0.5 \times r_{Cu,Fe}) \times r_{Cu,Cu}}{(0.5 \times r_{Cu,Sn} + 0.5 \times r_{Cu,Fe}) \times (1 - r_{Cu,Cu})} \quad (14)$$

Power was calculated based on the voltage drop across the external resistor, measured with a data acquisition system (PFN-2042 PROFINET, Hongge, Taiwan), as $P = I\,U$, where $I$ = current, and $U$ = voltage. Power density was normalized to the projected surface area of the separator, allowing comparison of the results to previous results.[35,45–46] CE was calculated as the ratio of the total coulombs calculated by integrating the current over time, and the theoretical amount of coulombs available based on the COD removed in the anodes of MFCs.[45–46]

## Acknowledgements

*The authors gratefully acknowledge financial support from the Natural Science Foundation of China (Nos. 51578104 and 21777017), the Open Project of State Key Laboratory of Urban Water Resource and Environment (No. HCK201706), and the Programme of Introducing Talents of Discipline to Universities (B13012).*

## Conflict of Interest

*The authors declare no conflict of interest.*

**Keywords:** microbial fuel cells · metal recovery · separation factor · Sn(II), Fe(II), Cu(II) · stainless-steel mesh

[1] M. S. Lee, J. G. Ahn, J. W. Ahn, *Hydrometallurgy* **2003**, *70*, 23–29.
[2] R. Buckle, S. Roy, *Sep. Purif. Technol.* **2008**, *62*, 86–96.
[3] M. Kumar Jha, P. Kumar Choubey, A. Kumari Jha, A. Kumari, J. C. Lee, V. Kumar, J. Jeong, *Waste Manage.* **2012**, *32*, 1919–1925.

[4] D. Orac, T. Havlik, A. Maul, M. Berwanger, *J. Min. Metall. Sect. B* **2015**, *51 B*, 153–161.
[5] M. A. H. Shuva, M. A. Rhamdhani, G. A. Brooks, S. Masood, M. A. Reuter, *J. Cleaner Prod.* **2016**, *131*, 795–809.
[6] M. Wang, Q. Tan, J. F. Chiang, J. Li, *Front. Environ. Sci. Eng.* **2017**, *11*, 1.
[7] I. Banerjee, B. Burrell, C. Reed, A. C. West, S. Banta, *Curr. Opin. Biotechnol.* **2017**, *45*, 144–155.
[8] S. H. Hamdan, G. F. Molelekwa, B. V. der Bruggen, *ChemElectroChem* **2014**, *1*, 1104–1117.
[9] X. Zhang, J. Guan, Y. Guo, X. Yan, H. Yuan, J. Xu, J. Guo, Y. Zhou, R. Su, Z. Guo, *ACS Sustainable Chem. Eng.* **2015**, *3*, 1696–1700.
[10] L. Meng, Y. Zhong, Z. Wang, K. Chen, X. Qiu, H. Cheng, Z. Guo, *ACS Sustainable Chem. Eng.* **2018**, *6*, 186–192.
[11] B. E. Logan, *ChemSusChem* **2012**, *5*, 988–994.
[12] T. H. J. A. Sleutels, A. Ter Heijne, C. J. N. Buisman, H. V. M. Hamelers, *ChemSusChem* **2012**, *5*, 1012–1019.
[13] Z. Wang, C. Cao, Y. Zheng, S. Chen, F. Zhao, *ChemElectroChem* **2014**, *1*, 1813–1821.
[14] M. Rahimnejad, A. Adhami, S. Darvari, A. Zirepour, S. E. Oh, *Alexandria Eng. J.* **2015**, *54*, 745–756.
[15] M. Mashkour, M. Rahimnejad, M. Mashkour, *J. Power Sources* **2016**, *325*, 322–328.
[16] M. Mashkour, M. Rahimnejad, M. Mashkour, G. Bakeri, R. Luque, S. E. Oh, *ChemElectroChem* **2017**, *4*, 1–8.
[17] M. Mashkour, M. Rahimnejad, M. Mashkour, G. Bakeri, R. Luque, S. E. Oh, *ChemElectroChem* **2017**, *4*, 648–654.
[18] G. Wang, L. Huang, Y. Zhang, *Biotechnol. Lett.* **2008**, *30*, 1959–1966.
[19] A. Ter Heijne, F. Liu, R. Van der Weijden, J. Weijma, C. J. N. Buisman, H. V. M. Hamelers, *Environ. Sci. Technol.* **2010**, *44*, 4376–4381.
[20] B. Zhang, C. Feng, J. Ni, J. Zhang, W. Huang, *J. Power Sources* **2012**, *204*, 34–39.
[21] Y. Zhang, L. Yu, D. Wu, L. Huang, P. Zhou, X. Quan, *J. Power Sources* **2015**, *273*, 1103–1113.
[22] D. Wu, L. Huang, X. Quan, G. Li Puma, *J. Power Sources* **2016**, *307*, 705–714.
[23] Q. Wang, L. Huang, Y. Pan, P. Zhou, X. Quan, B. E. Logan, H. Chen, *Bioresour. Technol.* **2016**, *200*, 565–571.
[24] Q. Wang, L. Huang, Y. Pan, X. Quan, G. Li Puma, *J. Hazard. Mater.* **2017**, *321*, 896–906.
[25] M. Li, Y. Pan, L. Huang, Y. Zhang, J. Yang, *Environ. Technol.* **2017**, *38*, 615–628.
[26] L. Huang, M. Li, Y. Pan, Y. Shi, X. Quan, G. Li Puma, *Chem. Eng. J.* **2017**, *327*, 584–596.
[27] Z. Wang, G. Dummi Mahadevan, Y. Wu, F. Zhao, *J. Power Sources* **2017**, *356*, 245–255.
[28] F. Zhang, M. D. Merrill, J. C. Tokash, T. Saito, S. Cheng, M. A. Hickner, B. E. Logan, *J. Power Sources* **2011**, *196*, 1097–1102.
[29] X. Zhang, D. Pant, F. Zhang, J. Liu, W. He, B. E. Logan, *ChemElectroChem* **2014**, *1*, 1859–1866.
[30] W. Yang, B. E. Logan, *ChemSusChem* **2016**, *9*, 2226–2232.
[31] K. Rabaey, S. Bützer, S. Brown, J. Keller, R. A. Rozendal, *Environ. Sci. Technol.* **2010**, *44*, 4315–4321.
[32] I. Gajda, J. Greenman, C. Melhuish, C. Santoro, I. Ieropoulos, *Bioresour. Technol.* **2016**, *215*, 285–289.
[33] O. Ichihashi, K. Hirooka, *Bioresour. Technol.* **2012**, *114*, 303–307.
[34] C. Abourached, T. Catal, H. Liu, *Water Res.* **2014**, *51*, 228–233.
[35] L. Huang, Y. Liu, L. Yu, X. Quan, G. Chen, *J. Cleaner Prod.* **2015**, *86*, 441–446.
[36] X. Li, Y. Zheng, P. Nie, Y. Ren, X. Wang, Y. Liu, *RSC Adv.* **2017**, *7*, 12503.
[37] I. Gajda, A. Stinchcombe, J. Greenman, C. Melhuish, I. Ieropoulos, *Int. J. Hydrogen Energy* **2017**, *42*, 1813–1819.
[38] Q. Wang, L. Huang, X. Quan, Q. Zhao, *Electrochim. Acta* **2017**, *247*, 880–890.
[39] Q. Wang, L. Huang, X. Quan, Q. Zhao, *J. Photochem. Photobiol. A* **2018**, *357*, 156–167.
[40] Y. Hong, D. F. Call, C. M. Werner, B. E. Logan, *Biosens. Bioelectron.* **2011**, *28*, 71–76.
[41] S. B. Pasupuleti, S. Srikanth, S. Venkata Mohan, D. Pant, *Int. J. Hydrogen Energy* **2015**, *40*, 12424–12435.
[42] W. Li, H. Yu, Z. He, *Energy Environ. Sci.* **2014**, *7*, 911–924.
[43] S. Gildemyn, R. A. Rozendal, K. Rabaey, *Trends Biotechnol.* **2017**, *35*, 393–406.
[44] H. Rismani-Yazdi, S. M. Carver, A. D. Christy, O. H. Tuovinen, *J. Power Sources* **2008**, *180*, 683–694.
[45] L. Huang, L. Gan, N. Wang, X. Quan, B. E. Logan, G Chen, *Biotechnol. Bioeng.* **2012**, *109*, 2211–2221.
[46] L. Huang, Y. Shi, N. Wang, Y. Dong, *Biodegradation* **2014**, *25*, 615–632.
[47] C. He, Z. Mu, H. Yang, Y. Wang, Y. Mu, H Yu, *Chemosphere* **2015**, *140*, 12–17.
[48] J. H. Adair, E. Suvaci, *Curr. Opin. Colloid Interface Sci.* **2000**, *5*, 160–167.
[49] M. Grattieri, N. D. Shivel, I. Sifat, M. Bestetti, S. D. Minteer, *ChemSusChem* **2017**, *10*, 2053–2058.
[50] K. K. Fedje, O. Modin, A. M. Stromvall, *Metals* **2015**, *5*, 1328–1348.
[51] L. Huang, Q. Wang, L. Jiang, P. Zhou, X. Quan, B. E. Logan, *Environ. Sci. Technol.* **2015**, *49*, 9914–9924.
[52] Y. V. Nancharaiah, S. Venkata Mohan, P. N. L. Lens, *Trends Biotechnol.* **2016**, *34*, 137–155.
[53] O. Modin, F. Aulenta, *Environ. Sci.-Water Res. Technol.* **2017**, *3*, 391–402.
[54] F. Harnisch, L. F. M. Rosa, F. Kracke, B. Virdis, J. O. Krömer, *ChemSusChem* **2015**, *8*, 758–766.
[55] G. Pasternak, J. Greenman, I. Ieropoulos, *ChemSusChem* **2016**, *9*, 88–96.
[56] Q. Li, J. Fu, W. Zhu, Z. Chen, B. Shen, L. Wu, Z. Xi, T. Wang, G. Lu, J. J. Zhu, S. Sun, *J. Am. Chem. Soc.* **2017**, *139*, 4290–4293.
[57] X. Zhang, N. Bao, K. Ramasamy, Y. H. A. Wang, Y. Wang, B. Lin, A. Gupta, *Chem. Commun.* **2012**, *48*, 4956–4958.
[58] C. Santoro, M. R. Talarposhti, M. Kodali, R. Gokhale, A. Serov, I. Merino-Jimenez, I. Ieropoulos, P. Atanassov, *ChemElectroChem* **2017**, *4*, 3322–3330.
[59] M. Rahimnejad, G. Bakeri, M. Ghasemi, A. Zirepour, *Polym. Adv. Technol.* **2014**, *25*, 1426–1432.
[60] K. R. Fradler, I. Michie, R. M. Dinsdale, A. Guwy, G. Premier, *Water Res.* **2014**, *55*, 115–125.
[61] B. E. Logan, M. J. Wallack, K. Y. Kim, W. He, Y. Feng, P. E. Saikaly, *Environ. Sci. Technol. Lett.* **2015**, *2*, 206–214.
[62] M. Rahimnejad, M. Ghasemi, G. D. Najafpour, M. Ismail, A. W. Mohammad, A. A. Ghoreyshi, S. H. A. Hassan, *Electrochim. Acta* **2012**, *85*, 700–706.
[63] M. Ghasemi, W. R. W. Daud, M. Ismail, M. Rahimnejad, A. F. Ismail, J. X. Leong, M. Miskan, K. B. Liew, *Int. J. Hydrogen Energy* **2013**, *38*, 5480–5484.
[64] Y. Qian, L. Huang, Y. Pan, X. Quan, H. Lian, J. Yang, *Sep. Purif. Technol.* **2018**, *192*, 78–87.
[65] Y. Song, X. Chen, Z. Zhao, L. Zhang, L. He, *Metall. Mater. Trans. B* **2016**, *47*, 675–685.

Manuscript received: April 2, 2018
Accepted Article published: April 21, 2018
Version of record online: May 11, 2018